Magnetoreflectance and magnetization of $Cu_2Zn_{1-x}Mn_xGeS_4$

O. W. Shih and R. L. Aggarwal*
Francis Bitter National Magnet Laboratory, Massachusetts Institute of Technology, Cambridge, Massachusetts 02139 and Department of Physics, Massachusetts Institute of Technology, Cambridge, Massachusetts 02139

T. Q. Vu and Y. Shapira†
Department of Physics, Tufts University, Medford, Massachusetts 02155

K. Doverspike,‡ R. N. Kershaw, K. Dwight, and A. Wold
Department of Chemistry, Brown University, Providence, Rhode Island 02912
(Received 9 January 1992)

We have measured the magnetoreflectance of orthorhombic $Cu_2Zn_{1-x}Mn_xGeS_4$ with $x = 0.83$, 0.92, and 1.00 at 1.3 K in applied dc magnetic fields **B** up to 15 T with **B** applied parallel to crystallographic directions **a**, **b**, and **c**. Exciton splittings as large as ~ 170 and ~ 230 meV were observed for light polarization vector $\mathbf{E} \parallel \mathbf{a}$ and $\mathbf{E} \parallel \mathbf{c}$, respectively. With increasing magnetic field, the average energy of the $\mathbf{E} \parallel \mathbf{a}$ exciton components decreased and that of the $\mathbf{E} \parallel \mathbf{c}$ components increased. Sample geometry did not permit $\mathbf{E} \parallel \mathbf{b}$ measurements. Room-temperature excitons were also observed but their Zeeman splittings were not observed. The excitons are associated with transitions between the conduction and valence bands, which were assumed to be *s* like and *p* like, respectively. We have also measured the magnetization of the $x = 0.92$ and 1.00 samples at 1.4 K in applied dc magnetic fields up to 19.5 T with $\mathbf{B} \parallel \mathbf{b}$. From the optical and magnetization data, we determined the *s-d* and *p-d* exchange constant difference $N_0\alpha - N_0\beta$ where $N_0\alpha$ and $N_0\beta$ measure the exchange interaction between the Mn^{2+} $3d$ electrons and the conduction- and valence-band electrons, respectively. For $x = 0.92$, we obtained $N_0\alpha - N_0\beta_x = 0.089 \pm 0.005$ eV and $N_0\alpha - N_0\beta_z = 0.126 \pm 0.007$ eV. For $x = 1.00$, we obtained $N_0\alpha - N_0\beta_x = 0.077 \pm 0.005$ eV and $N_0\alpha - N_0\beta_z = 0.110 \pm 0.007$ eV. These values are an order of magnitude smaller than those observed in II-VI diluted magnetic semiconductors.

I. INTRODUCTION

In Mn-based II-VI diluted magnetic semiconductors (DMS's),[1] antiferromagnetic (AF) interactions between the Mn^{2+} ions reduce the magnetization attainable in magnetic fields $B \lesssim 20$ T.[2] The Mn^{2+} ions are coupled together into clusters necessitating very large magnetic fields to achieve saturation magnetization. For example, the saturation of Mn^{2+} pairs in $Cd_{0.905}Mn_{0.095}Te$ at $T \sim 4$ K occurs at $B \sim 52$ T.[3] Total magnetization saturation of $Cd_{0.9}Mn_{0.1}Te$ at ~ 10 K occurs at 80 T.[4] As discussed by Heiman *et al.*,[5] since the Mn^{2+}-Mn^{2+} exchange interaction grows weaker with distance, the Mn^{2+} ions coupled most strongly by the AF interaction occupy nearest-neighbor sites. Therefore, the magnetization may be enhanced by decreasing the number of nearest-neighbor sites and increasing the distance between the magnetic ions.

To find materials satisfying these conditions, Wolff and Ram-Mohan[6] proposed the study of DMS's derived from I_2-II-IV-VI_4 compounds with the stannite or wurtz-stannite structures.[7–10] One example is $Cu_2Zn_{1-x}Mn_xGeS_4$ which has the orthorhombic wurtz-stannite structure; when $x = 1$, the effective magnetic-ion concentration is 1/4. In this class of tetrahedrally bonded, diamond-type crystals, magnetic ions like Mn^{2+} occupying sites in the group-II cation sublattice do not have other magnetic ions as nearest neighbors. In contrast, a magnetic ion in a II-VI DMS like $Cd_{1-x}Mn_xTe$ may have up to 12 magnetic ions as nearest neighbors. Furthermore the shortest distance between two Mn^{2+} ions in Cu_2MnGeS_4, for example, is approximately equal to the distance between *next-nearest* neighbors in $Cd_{1-x}Mn_xTe$.

In the case of $Cu_2Zn_{1-x}Mn_xGeS_4$, the expected enhancement in magnetization has been experimentally verified by Shapira *et al.*[11] For $x = 1$ and $B \sim 20$ T, they observed a maximum magnetization which is an order of magnitude larger than that achieved in II-VI DMS's at $B \sim 20$ T. Also the observed saturation field $B \simeq 18$ T at 1.3 K is relatively low. This confirms that the Mn^{2+}-Mn^{2+} AF interactions are weaker than those in Mn-based II-VI DMS's.

In this paper, we look at another aspect of DMS's derived from I_2-II-IV-VI_4 compounds. Instead of interactions between magnetic ions, we investigate the exchange interaction between the localized electrons of the magnetic ions and the band electrons which is responsible for the unusually large magneto-optical effects in DMS's. Optical, electrical, and magnetic characteristics of I_2-II-

IV-VI_4 compounds have been previously reported.[11–16]

We report the results of magnetoreflectance measurements in $Cu_2Zn_{1-x}Mn_xGeS_4$. We present magnetoreflectance measurements of exciton splittings for $x = 0.83$, 0.92, and 1.00 measured at 1.3 K in magnetic fields up to 15 T. We also present magnetization curves for $x = 0.92$ and 1.00 measured at 1.4 K in magnetic fields up to 19.5 T. From the optical and magnetic data, we determined values for the exchange constant difference $N_0\alpha - N_0\beta$ where $N_0\alpha$ and $N_0\beta$ are measures of the coupling strength between the ion and conduction-band electrons and between the ion and valence-band electrons, respectively. We find that $N_0\alpha - N_0\beta$ is an order of magnitude *smaller* than that observed in II-VI DMS's.

II. EXPERIMENT

A. Crystals

Single crystals of $Cu_2Zn_{1-x}Mn_xGeS_4$ with nominal compositions $x = 0.83$, 0.90, and 1.00 were grown by chemical vapor transport as described in Ref. 17. Chemical probe analysis indicated that the $x = 0.90$ crystal had a Mn concentration of $x = 0.92$. The crystals had the form of small flat thin rectangular platelets whose approximate dimensions are given in Table I. Samples with $x = 1.00$ and 0.92 were black in color but appeared red when held up to the light. The sample with $x = 0.83$ was so thin that it always appeared red. The as-grown crystal surfaces appeared smooth and reflecting but not mirrorlike and were neither polished nor etched for the reflectance measurements.

The orientation of the orthorhombic crystallographic directions **a**, **b**, and **c** was determined by comparing back-reflection Laue photographs with computer generated Laue plots.[18] [Equation (6.1) in Ref. 18 is incorrect; the correct form is given below in the Appendix.] With the x-ray beam normal to the platelet surface, Laue photos for all three samples displayed a twofold symmetry pattern. Theoretical Laue plots were calculated using Cu_2MnGeS_4 lattice constants.[10] For all three x compositions, we determined that **c**, **a**, and **b** were parallel to the long edge, short edge, and normal of the crystal platelets.

B. Techniques

Magnetoreflectance spectra were recorded with the samples immersed in pumped liquid helium at 1.3 K and in applied dc magnetic fields B up to 15 T. The magnetic field was oriented $\mathbf{B} \parallel \mathbf{a}$, $\mathbf{B} \parallel \mathbf{b}$, and $\mathbf{B} \parallel \mathbf{c}$, and for each orientation the electric field was linearly polarized $\mathbf{E} \parallel \mathbf{a}$ and $\mathbf{E} \parallel \mathbf{c}$ with light propagation vector $\mathbf{k} \parallel \mathbf{b}$ in all cases.

The major components of our apparatus were a GE#T8-1/2 tungsten lamp source, a 0.22-m Spex double-grating monochromator model 1680B equipped with 1200 grooves/mm gratings blazed at 500 nm, a Polaroid HN38 linear polarizer, an RCA#4382 photomultiplier detector, and a Princeton Applied Research lock-in amplifier model 5101. Both monochromator slits were set at 100 μm giving a spectral resolution of 0.3 nm. The spectra were recorded by sweeping the wavelength of the monochromator at fixed values of B. The spectra were then divided by the appropriate reference spectrum obtained separately by substituting a front-surface aluminum mirror in place of the DMS crystal.

The magnetization of the same crystals used in the optical experiments were measured at 1.4 K in applied dc magnetic fields $\mathbf{B} \parallel \mathbf{b}$ up to 19.5 T using a vibrating-sample magnetometer. The magnetization curve of the $x = 0.83$ crystal is omitted here since the sample's low mass ($\sim$ 1 mg) did not permit reliable measurements.

III. RESULTS

A. Magnetoreflectance

1. $B = 0$

Figure 1(a) shows $B = 0$ reflectance spectra for the $x = 1.00$ and 0.92 samples measured at room temperature. The $x = 0.83$ sample was destroyed during a magnetization measurement and was unavailable for a room-temperature measurement. The square and triangle symbols indicate $\mathbf{E} \parallel \mathbf{a}$ and $\mathbf{E} \parallel \mathbf{c}$ polarizations, respectively, and also the exciton transition energies recorded. The size of the exciton features for both $x = 0.92$ and 1.00 was $\Delta R/R \sim 0.05$ where ΔR is the difference in reflectance between the top and bottom of the negatively sloped portion of the exciton and R is the average of the two reflectances. Figure 1(b) shows the $B = 0$ exciton spectra for all three samples measured at 1.3 K. For $x = 0.83$, 0.92, and 1.00, $\Delta R/R \sim 0.06$, 0.07, and 0.15 respectively. Table I summarizes the exciton transition energies recorded from these two figures. Upon cooling from 300 to 1.3 K, the exciton transition energies increased by about 100 meV. The change in band-gap energy E_g with temperature is $dE_g/dT < 0$ which is the

TABLE I. $Cu_2Zn_{1-x}Mn_xGeS_4$ sample dimensions and $B = 0$ exciton transition energies measured at 300 and 1.3 K.

x	$l \times w \times h$ (mm)	$\mathbf{E} \parallel \mathbf{a}$ (300 K) (eV)	$\mathbf{E} \parallel \mathbf{c}$ (300 K) (eV)	$\mathbf{E} \parallel \mathbf{a}$ (1.3 K) (eV)	$\mathbf{E} \parallel \mathbf{c}$ (1.3 K) (eV)
1.00	4×2×0.2	2.293 ± 0.02	2.419 ± 0.01	2.412 ± 0.003	2.531 ± 0.004
0.92	3×2×1	2.231 ± 0.01	2.381 ± 0.01	2.330 ± 0.004	2.478 ± 0.004
0.83	3×2×0.05	a	a	2.301 ± 0.005	2.468 ± 0.005

[a]Not available.

usual behavior in semiconductors. In general, the low- and high-energy transitions were obtained for **E** || **a** and **E** || **c** polarizations, respectively. The energy difference between the low- and high-energy transitions represents the crystal-field splitting $\Delta E_{\text{c-f}}$ between two levels of the valence band (assuming that the conduction band is *s*-like as discussed in Sec. IV).

As Mn concentration x decreases, the crystal-field splitting increases. This is correlated with the distortion of the $Cu_2Zn_{1-x}Mn_xGeS_4$ lattice away from the ideal wurtzite lattice.[19] The relationships between the ideal orthorhombic and wurtzite lattice constants are[10] $a_{\text{ortho}} = 2\,a_{\text{wurt}}$, $b_{\text{ortho}} = \sqrt{3}\,a_{\text{wurt}}$, and $c_{\text{ortho}} = c_{\text{wurt}}$, where c_{wurt} is parallel to the sixfold symmetry axis. Also, for ideal wurtzite, $c_{\text{wurt}} = 2\sqrt{2/3}\,a_{\text{wurt}}$. Table II lists the actual lattice constants,[10] the ideal lattice constants, and the fractional distortion from ideal for Cu_2MnGeS_4 and Cu_2ZnGeS_4. Also listed are the experimentally measured crystal-field splittings at 1.3 K. We see that the crystal-field splitting increases as fractional distortion increases.

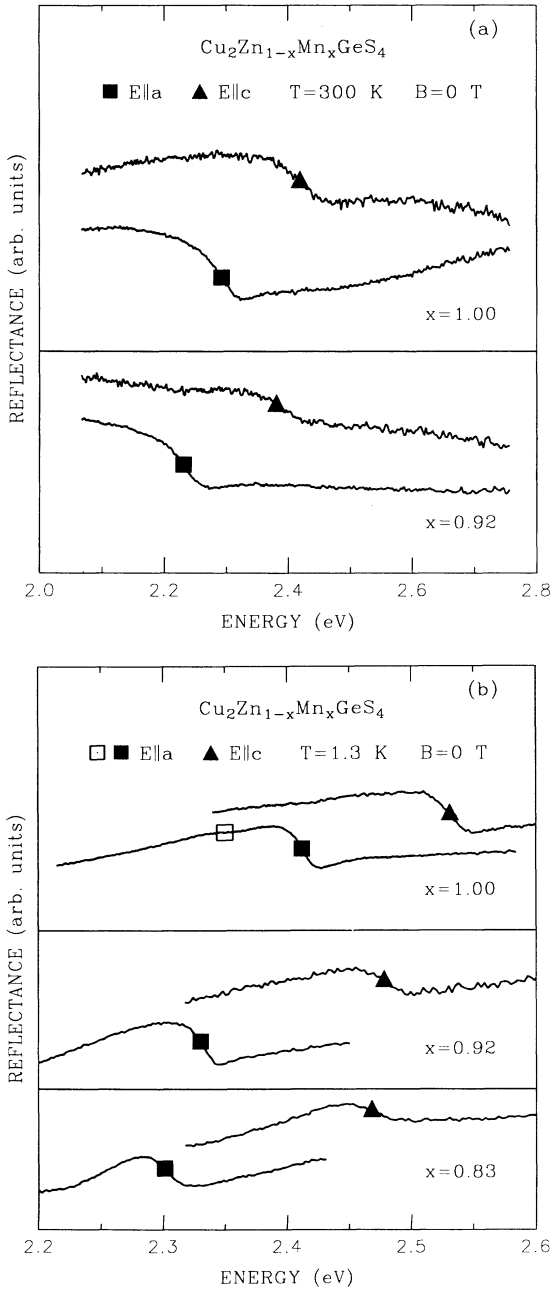

FIG. 1. $Cu_2Zn_{1-x}Mn_xGeS_4$ reflectance spectra measured at $B = 0$ and at (a) 300 K and (b) 1.3 K. The square and triangle symbols indicate **E** || **a** and **E** || **c** polarizations, respectively, and also the exciton transition energies recorded.

The observation of excitons at room temperature implies that the binding energy is greater than 25 meV. At 1.3 K the exciton widths are ~ 30 meV which is approximately ten times wider than that observed for II-VI based DMS's.[20–22] At 300 K the exciton widths increase to ~ 60 meV. The large widths at low temperatures imply that the samples probably have many scattering centers which increase the exciton widths and thereby dominate the natural intrinsic exciton widths which probably are much narrower. When the temperature increases from $T_i = 1.3$ K to $T_f = 300$ K, the exciton widths increase by $\sim k_B(T_f - T_i)$. This suggests that the exciton binding energy is of order several $k_B(T_f - T_i)$, i.e., of order 100 meV; otherwise, the excitons would have broadened too much to be observed. Furthermore, the widths of the **E** || **a** and **E** || **c** excitons which are ~ 120 meV apart are approximately the same. This too suggests a fairly large binding energy of order 100 meV.

An estimate of the exciton reduced mass μ_r may be obtained from the above estimate of the binding energy using the expression for the binding energy E_b of the ground-state exciton,[23] $E_b = -(\mu_r q^4)/(2\hbar^2\epsilon^2)$, where q is the electron charge and ϵ is the dielectric constant. In Ref. 13, the average refractive index n is given for several I_2-II-IV-VI_4 compounds, although for neither Cu_2ZnGeS_4 nor Cu_2MnGeS_4. However, the values of n range from 2.33 to 2.85. Assuming that our crystals have similar indices of refraction, we chose an average value $n \simeq 2.5$. Then approximating $\epsilon \simeq n^2$ and $|E_b| \sim 100$ meV, we obtained the exciton reduced mass $\mu_r/m_e \sim 0.29$ and the radius of the ground-state exciton orbit $a_{\text{exciton}} \sim 11.4$ Å, which shows that the exciton orbit encompasses relatively few lattice sites compared to that in II-VI DMS's.

2. $B \neq 0$

Magnetoreflectance spectra were measured for all three samples at 1.3 K. For each sample, the magnetic field was oriented along each of the crystallographic directions **a**, **b**, and **c**. For each magnetic-field orientation, **E** was linearly polarized parallel to **a** and to **c**. The spectra were all qualitatively alike. Figure 2(a) shows representative $Cu_2Zn_{1-x}Mn_xGeS_4$ ($x = 1.00$) magnetoreflectance spectra measured for **B** || **c** and **E** || **a** at 1.3 K for several B-values. At $B = 0$, a relatively strong exciton was observed at 2.41 eV and a much weaker exciton at 2.35 eV. The weaker exciton was observed only with the $x = 1.00$ sample and represents an unidentified transition. We associated the stronger exciton with the valence-band to conduction-band transition.

TABLE II. $Cu_2Zn_{1-x}Mn_xGeS_4$ lattice constants (a, b, c), fractional distortion from ideal wurtzite structure, and crystal-field splittings $\Delta E_{c\text{-}f}$ measured at 1.3 K. $\Delta E_{c\text{-}f}$ increases as lattice distortion from the ideal wurtzite structure increases.

x	Actual (a, b, c) (Å)	Ideal (a, b, c) (Å)	Fractional distortion a axis	b axis	$\Delta E_{c\text{-}f}$ (eV)
1.00	(7.608, 6.511, 6.236) [a]	(7.638, 6.614, 6.236)	−0.0039	−0.0156	0.119
0.92					0.148
0.83					0.167
0.00	(7.504, 6.474, 6.185) [a]	(7.575, 6.614, 6.185)	−0.0094	−0.0212	

[a]Reference 10.

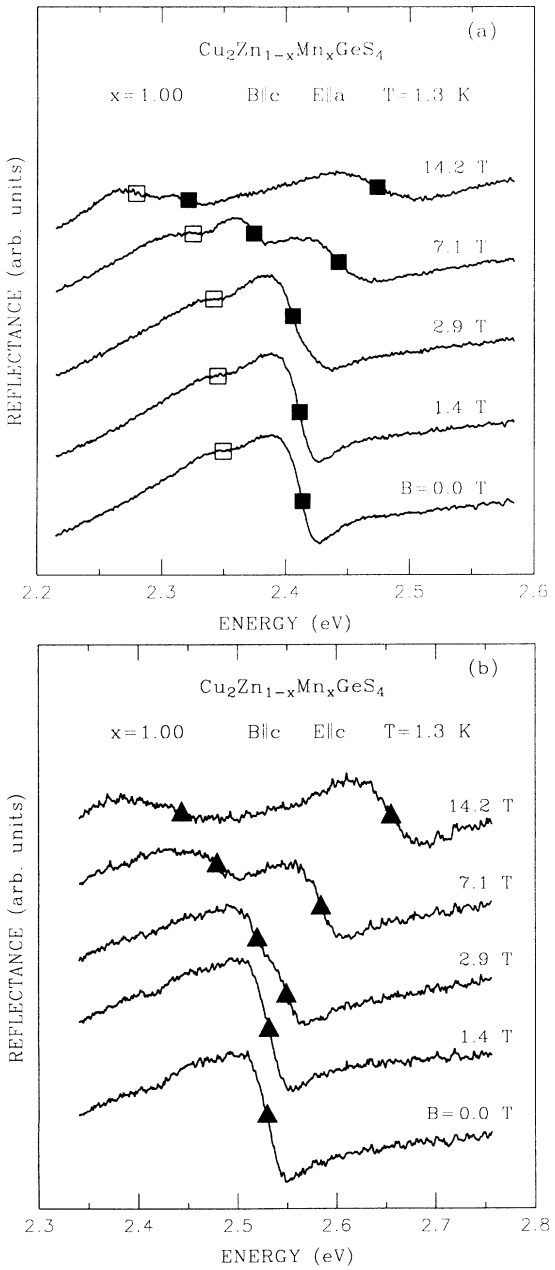

FIG. 2. $Cu_2Zn_{1-x}Mn_xGeS_4$ (x = 1.00) magnetoreflectance spectra measured at 1.3 K for **B** || **c**. (a) **E** || **a**. Square symbols indicate exciton transition energies. The open squares indicate an unidentified transition observed only for the x = 1.00 sample. (b) **E** || **c**. Triangle symbols indicate exciton transition energies.

At B = 1.4 T, the exciton line-shape and transition energies remained practically the same. At B = 2.9 T, the line shape of the stronger exciton became broader but the transition energies remained unchanged. At B = 7.1 T, the stronger exciton had split into two components at 2.37 and 2.44 eV. The weaker exciton had moved down slightly to 2.33 eV. At B = 14.2 T, the two components of the stronger exciton had split further apart to 2.32 and 2.47 eV. The weaker exciton, which had moved further down to 2.28 eV, appeared to remain as a single exciton.

Figure 2(b) shows representative $Cu_2Zn_{1-x}Mn_xGeS_4$ (x = 1.00) magnetoreflectance spectra measured for **B** || **c** and **E** || **c** at 1.3 K for several B values. At B = 0, a single exciton was observed at 2.53 eV. At B = 1.4 T, no splitting of the exciton was resolved which remained at 2.53 eV. At B = 2.9 T, the two components of the exciton could just be resolved at 2.52 and 2.55 eV. At B = 7.1 T, the exciton components had split further apart to 2.48 and 2.58 eV. At B = 14.2 T, the transition energies of the two components were 2.44 and 2.66 eV. We note that the low-energy components had a broader line shape than the high-energy components. This is in contrast to the II-VI DMS's in which the opposite occurs.

The magnetoreflectance spectra taken at $B \simeq 15$ T for all three samples were qualitatively similar and are shown in Fig. 3. In the presence of a magnetic field, the **E** || **a** and **E** || **c** excitons were each observed to split into two components. The energy difference between the low- and high-energy components at 15 T is given in Table III. The exciton splitting did not decrease linearly with decreasing x. Rather it appeared to increase slightly as x changed from 1.00 to 0.92. Only for x = 0.83 did the splitting noticeably decrease.

Figure 4 shows a plot of the $Cu_2Zn_{1-x}Mn_xGeS_4$ (x = 1.00) exciton transition energies for the **B** || **c** orientation and for both **E**-field polarizations as a function of magnetic field. The error bars indicate the uncertainty in determining the transition energies by eye due to the exciton widths. Included is the unidentified transition which was seen quite clearly for the **B** || **b** and **B** || **c** orientations. Noise obscured this transition for **B** || **a**.

The exciton transition energies vs B for each sample for all three B-field orientations are plotted in Fig. 5. The exciton splittings for the three B-field orientations for a given **E**-field polarization coincide very well. The reason is that $Cu_2Zn_{1-x}Mn_xGeS_4$ is a low-anisotropy antiferromagnet.[11] The magnetization of $Cu_2Zn_{1-x}Mn_xGeS_4$ does not depend strongly on the direction of the magnetic field. Another feature concerns

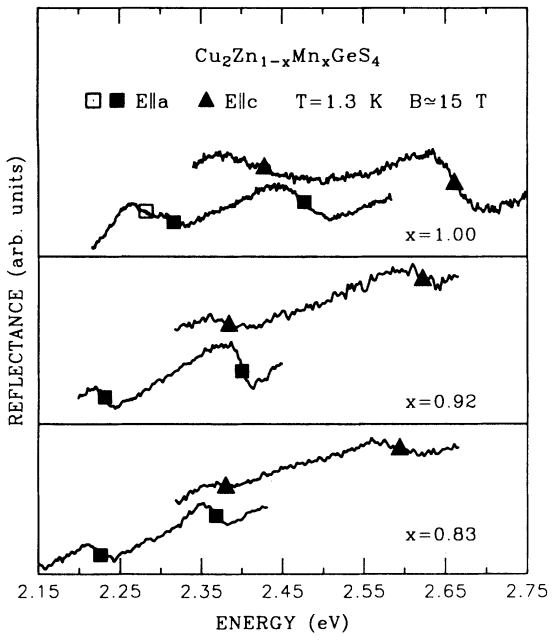

FIG. 3. $Cu_2Zn_{1-x}Mn_xGeS_4$ magnetoreflectance **B** || **c** spectra measured at 1.3 K and 15 T for $x = 0.83$, 0.92, and 1.00. The square and triangle symbols indicate the exciton transition energies recorded in the **E** || **a** and **E** || **c** polarizations respectively. The open square symbol indicates the unidentified transition observed only with the $x = 1.00$ sample.

selection rules. The low-energy exciton was always obtained for **E** || **a** and the high-energy transition was always obtained for **E** || **c** regardless of magnetic-field direction. Thus, light polarization with respect to the crystallographic axes and not with respect to the magnetic field determined which transition was observed.

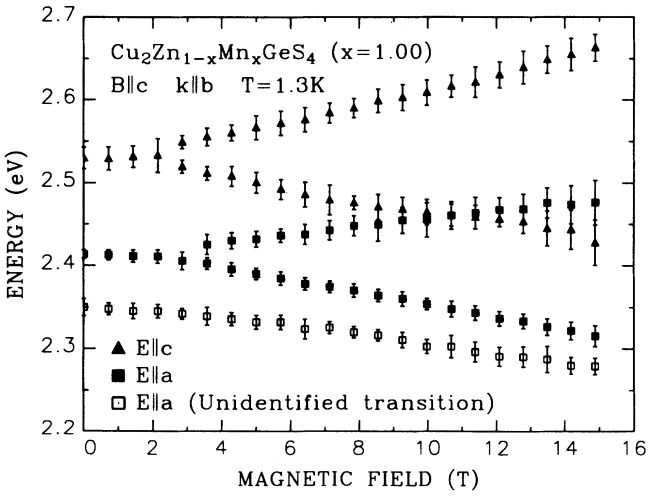

FIG. 4. $Cu_2Zn_{1-x}Mn_xGeS_4$ ($x = 1.00$) exciton transition energies vs B for **B** || **c**. The polarizations and transition energies are indicated by the square and triangle symbols in accordance with Fig. 2.

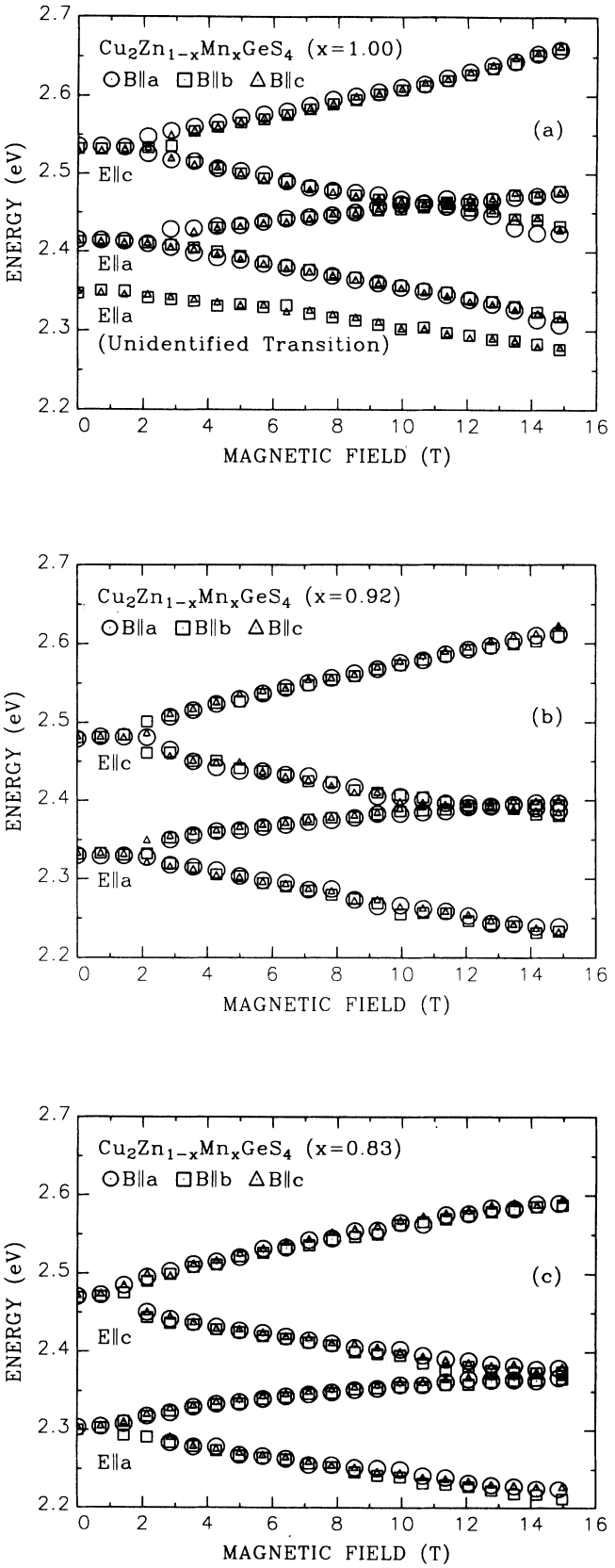

FIG. 5. $Cu_2Zn_{1-x}Mn_xGeS_4$ exciton transition energies vs B at 1.3 K. (a) $x = 1.00$. (b) $x = 0.92$. (c) $x = 0.83$.

TABLE III. Splitting difference between low- and high-energy exciton components measured in $Cu_2Zn_{1-x}Mn_xGeS_4$ at 1.3 K and 15 T.

x	**E** ∥ **a** (eV)	**E** ∥ **c** (eV)
1.00	0.161 ± 0.012	0.233 ± 0.032
0.92	0.169 ± 0.006	0.238 ± 0.010
0.83	0.142 ± 0.009	0.214 ± 0.014

Although excitons were observed at 300 K, no exciton splitting was observed in B fields up to 15 T. We may understand why as follows. For Cu_2MnGeS_4, which has a Néel temperature of $T_N = 8.25$ K,[11] the magnetization at 300 K may be modeled by a Brillouin function. At $B = 15$ T and $T = 300$ K, the magnetization would be ~ 7.8% of saturation value or ~ 5.5 emu/g. At $B = 15$ T and $T = 1.3$ K, the measured magnetization is ~ 60 emu/g. Thus a temperature increase from 1.3 to 300 K would cause the magnetization to drop by a factor of 11. Consequently the exciton splitting would drop by a factor of 11. The largest splitting observed at 1.3 K is about 230 meV. Thus the splitting at room temperature would be about 20 meV. However, the smallest splitting resolvable is of the order of the exciton width. At room temperature, the exciton width is about 60 meV which implies that the smallest splitting resolvable exceeds the predicted room-temperature splitting by a factor of 3. Thus the exciton width is too wide and the magnetization is too small for room-temperature exciton splitting to be observed.

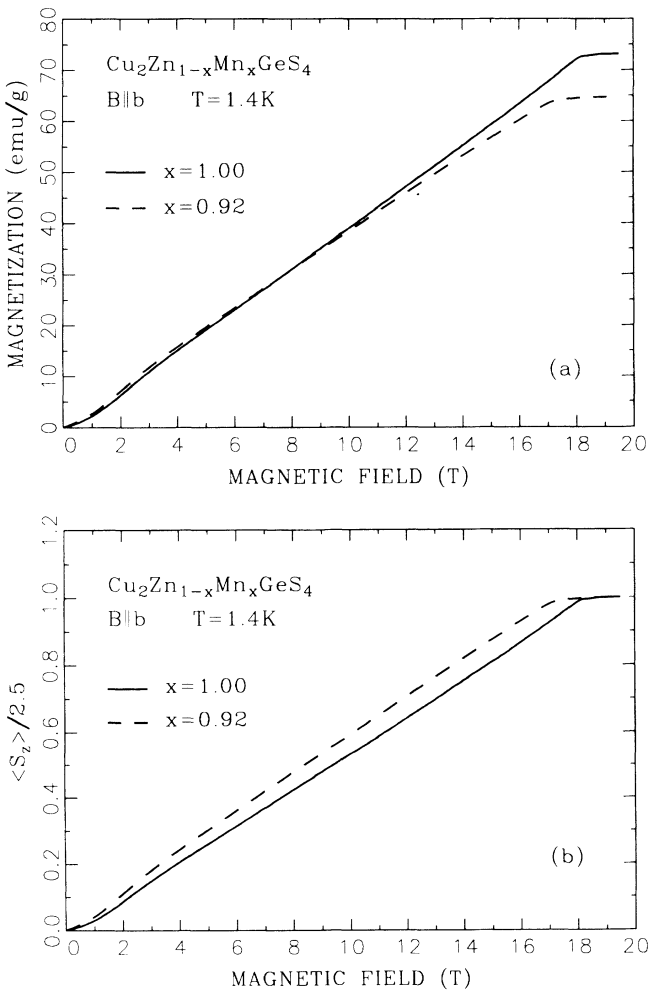

FIG. 6. (a) Magnetization and (b) average Mn^{2+} ion spin $|\langle S\rangle|$ vs B in $Cu_2Zn_{1-x}Mn_xGeS_4$ measured at 1.4 K for **B** ∥ **b**.

B. Magnetization

Figure 6(a) shows the measured magnetization vs B for the $x = 1.00$ and 0.92 samples with the magnetic field **B** ∥ **b**. The $x = 0.83$ sample had insufficient mass for a meaningful measurement. As discussed in Ref. 11, the magnetization is linear with B except at low fields, $B \leq 2$ T, and at high fields, $B = 17$–18 T, which is indicative of a low-anisotropy antiferromagnet. The low-field behavior is associated with the rotation of the magnetic-ion spins from their equilibrium $B = 0$ orientation to a nearly perpendicular-to-**B** orientation. The linear portion is associated with the tipping of the sublattice magnetizations towards the **B**-field direction. The plateau at high fields is associated with the sublattice magnetizations being parallel to **B**. At this point, the magnetization has reached maximum value and thus remains constant.

The measured magnetization M and the average magnetic-ion spin $|\langle S\rangle|$ along **B** are related by[21]

$$M = \frac{N_A \mu_B g_{\text{ion}}}{W} x |\langle S\rangle|, \tag{1}$$

where N_A is Avogadro's number, g_{ion} is the Mn^{2+} ion g factor, and W is the molecular weight of the crystal. The maximum magnetization is obtained by setting $|\langle S\rangle| = 5/2$ and $g_{\text{ion}} = 2$ (Ref. 11). The calculated maximum magnetizations are 72.9 and 66.9 emu/g for the $x = 1.00$ and 0.92 samples, respectively, which agree well with the respective experimental values 73.2 and 64.8 emu/g.

Figure 6(b) shows the average Mn^{2+} spin $|\langle S\rangle|$ obtained from the magnetization. Even in the wurtz-stannite structure, AF interactions act to reduce $|\langle S\rangle|$ with increasing x. For $x \leq 0.1$, $|\langle S\rangle|$ would have the form of a modified Brillouin function.[11]

IV. DISCUSSION

Figure 7 shows the model for the electronic energy levels and exciton transitions suggested by the optical data. This model is based upon two assumptions. First, the conduction and valence bands are assumed to be s-like and p-like, respectively. (To our knowledge, the band structure of $Cu_2Zn_{1-x}Mn_xGeS_4$ has not been published.) We infer this from the crystal structure's tetrahedral bonding arrangement which arises from s-p^3 hybridization.[7] There may be some p-d hybridization,

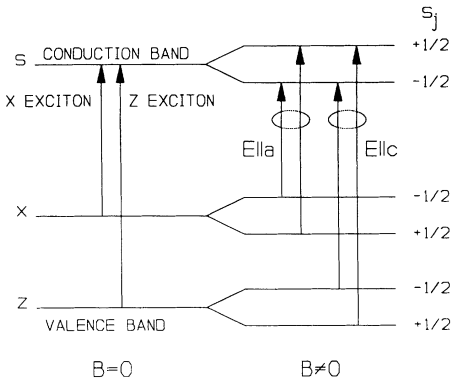

FIG. 7. $Cu_2Zn_{1-x}Mn_xGeS_4$ energy-level diagram and exciton transitions drawn for the case $N_0\alpha > 0$ and $N_0\beta < 0$. The $\mathcal{Y}$ levels are not drawn. Coordinate axes (x, y, z) correspond to crystal axes (a, b, c).

but it is not considered here. The s-like and p-like energy bands involved in the optical transitions shall be represented by the periodic functions $\mathcal{S}$, $\mathcal{X}$, $\mathcal{Y}$, and $\mathcal{Z}$ which have the same symmetry properties as the atomic functions s, p_x, p_y, and p_z.

The second assumption is that spin-orbit splitting is very much less than the crystal-field splitting and thus may be neglected. We infer this from the $B = 0$ spectra which exhibit one transition for $\mathbf{E} \parallel \mathbf{a}$ and a distinctly different transition for $\mathbf{E} \parallel \mathbf{c}$. The energy of the transition depends strongly on the orientation of the polarization with respect to the crystallographic axes. This suggests that the orbital angular momentum of the p states is sufficiently quenched to render the spin-orbit interaction negligible. Thus the splitting between the $\mathcal{X}$ and $\mathcal{Z}$ levels of the valence band shown in Fig. 7 is attributed solely to the orthorhombic crystalline symmetry of Cu_2ZnGeS_4 and Cu_2MnGeS_4 which is described by the space group C_{2v}^7 $(Pmn2_1)$.[9,10] The remaining twofold electron spin degeneracy is lifted for $B \neq 0$. The $+1/2$ and $-1/2$ spin eigenfunctions shall be represented by the symbols $\uparrow$ and $\downarrow$, respectively.

In contrast, the II-VI DMS's having cubic or hexagonal crystal symmetry often have strong spin-orbit interactions which cannot be ignored. In the valence band, the orbital and spin angular momenta couple together to form fourfold and twofold degenerate energy bands. In $Cu_2Zn_{1-x}Mn_xGeS_4$, the orbital and spin angular momenta remain uncoupled.

The transitions between the $\mathcal{X}$ and $\mathcal{Z}$ valence bands and the $\mathcal{S}$ conduction band drawn in Fig. 7 model the excitons observed in our experiments. Since the low- and high-energy transitions are obtained for $\mathbf{E} \parallel \mathbf{a}$ and $\mathbf{E} \parallel \mathbf{c}$ polarizations, respectively, the $\mathcal{X}$ level is drawn nearer to the conduction band than the $\mathcal{Z}$ level. Since $\mathbf{E} \parallel \mathbf{b}$ polarization was not possible with our crystals, the position of the $\mathcal{Y}$ level is omitted in the figure.

The signs of $N_0\alpha$ and $N_0\beta$ cannot be determined from our measurements. However, in all Mn-based wide-gap II-VI DMS's studied so far, $N_0\alpha$ has always been positive and $N_0\beta$ negative. For this reason, Fig. 7 is drawn with $N_0\alpha > 0$ and $N_0\beta < 0$. This need not necessarily be the correct choice. Also, the transitions have been drawn such that spin is conserved. This may be understood by recalling that the electric-dipole operator which induces the optical transitions acts only on the spatial part of the basis functions and leaves the spin part unaffected.

With the above assumptions, the Hamiltonian has the form

$$H = H_0 + H_{\text{exch}}, \tag{2}$$

where H_0 represents the kinetic energy and the crystal potential and H_{exch} represents the sp-d exchange interaction. We adopted the form of H_{exch} commonly used to analyze II-VI DMS's. In the molecular-field and virtual-crystal approximations, H_{exch} is written

$$H_{\text{exch}} = -x\, s\, \langle S\rangle \sum_{\mathbf{R}} J(\mathbf{r} - \mathbf{R}), \tag{3}$$

where s and $\langle S\rangle$ are, respectively, the components of the electron spin and average magnetic-ion spin along $\mathbf{B}$, $J(\mathbf{r} - \mathbf{R})$ is the electron-ion exchange coupling "constant," $\mathbf{r}$ is the band electron position coordinate, and the sum is over all group-II lattice sites $\mathbf{R}$. We used as basis states the direct products $\mathcal{S}\otimes(\uparrow, \downarrow)$ for the conduction band and $(\mathcal{X}, \mathcal{Y}, \mathcal{Z})\otimes(\uparrow, \downarrow)$ for the valence band.

The conduction- and valence-band matrices are diagonal. The conduction-band energy $E_{s\uparrow}$ is

$$E_{s\uparrow} \equiv \langle \mathcal{S}\uparrow | H_0 + H_{\text{exch}} | \mathcal{S}\uparrow\rangle \tag{4a}$$

$$= \langle \mathcal{S}\uparrow | \mathcal{H}_0 | \mathcal{S}\uparrow\rangle + \langle \mathcal{S}\uparrow | -xs\langle S\rangle \sum_{\mathbf{R}} J(\mathbf{r} - \mathbf{R}) | \mathcal{S}\uparrow\rangle, \tag{4b}$$

$$= E_s - x\tfrac{1}{2}N_0\alpha\langle S\rangle, \tag{4c}$$

$$= E_s + x\tfrac{1}{2}N_0\alpha|\langle S\rangle|, \tag{4d}$$

where N_0 is the number of unit cells per unit volume. The relation $\langle S\rangle = -|\langle S\rangle|$ substituted into Eq. (4c) comes from the antiparallel orientation of the spin and magnetic moment directions. Similarly,

$$E_{x\uparrow} = E_x + x\tfrac{1}{2}N_0\beta_x|\langle S\rangle|, \tag{5}$$

$$E_{y\uparrow} = E_y + x\tfrac{1}{2}N_0\beta_y|\langle S\rangle|, \tag{6}$$

$$E_{z\uparrow} = E_z + x\tfrac{1}{2}N_0\beta_z|\langle S\rangle|, \tag{7}$$

where the following parameters are defined: the conduction- and valence-band energies

$$E_s = \langle \mathcal{S}|H_0|\mathcal{S}\rangle, \tag{8a}$$

$$E_x = \langle \mathcal{X}|H_0|\mathcal{X}\rangle, \tag{8b}$$

$$E_y = \langle \mathcal{Y}|H_0|\mathcal{Y}\rangle, \tag{8c}$$

$$E_z = \langle \mathcal{Z}|H_0|\mathcal{Z}\rangle, \tag{8d}$$

and the sp-d exchange constants

$$\alpha = \langle \mathcal{S}|J(\mathbf{r})|\mathcal{S}\rangle, \tag{9a}$$

$$\beta_x = \langle \mathcal{X}|J(\mathbf{r})|\mathcal{X}\rangle, \tag{9b}$$

$$\beta_y = \langle \mathcal{Y}|J(\mathbf{r})|\mathcal{Y}\rangle, \tag{9c}$$

$$\beta_z = \langle \mathcal{Z}|J(\mathbf{r})|\mathcal{Z}\rangle. \tag{9d}$$

The energies $E_{s\downarrow}$, $E_{x\downarrow}$, $E_{y\downarrow}$, and $E_{z\downarrow}$, are obtained by changing the plus signs to minus signs in Eqs. (4d)–(7). By symmetry the crystal-field energies and exchange constants are anisotropic. The quantity $x|\langle S\rangle|$ is obtained from the experimentally measured magnetization using Eq. (1). The x values are the actual Mn concentrations, i.e., $x = 0.83$, 0.92, and 1.00, not the effective concentration $x_{\text{eff}} = x/4$.

The values of the *sp-d* parameters are determined by fitting expressions for the exciton splittings to experimental data. From Fig. 7, the **E** || **a** transition energies are

$$E_{a\uparrow} \equiv E_{s\uparrow} - E_{x\uparrow}, \tag{10a}$$
$$= (E_s - E_x) + \tfrac{1}{2}x|\langle S\rangle|(N_0\alpha - N_0\beta_x) \tag{10b}$$

and

$$E_{a\downarrow} \equiv E_{s\downarrow} - E_{x\downarrow}, \tag{11a}$$
$$= (E_s - E_x) - \tfrac{1}{2}x|\langle S\rangle|(N_0\alpha - N_0\beta_x). \tag{11b}$$

The energy difference between the two components of the exciton is

$$\Delta E_a \equiv E_{a\uparrow} - E_{a\downarrow}, \tag{12a}$$
$$= x|\langle S\rangle|(N_0\alpha - N_0\beta_x). \tag{12b}$$

Similarly, for the **E** || **c** transition,

$$\Delta E_c \equiv E_{c\uparrow} - E_{c\downarrow}, \tag{13a}$$
$$= x|\langle S\rangle|(N_0\alpha - N_0\beta_z). \tag{13b}$$

$N_0\alpha - N_0\beta$ is an algebraic quantity where $N_0\alpha$ and $N_0\beta$ may each be either positive or negative.

A least-squares fit of Eqs. (12b) and (13b) to the optical splitting data is plotted in Fig. 8. For the $x = 1.00$ sample, we obtained

$$N_0\alpha - N_0\beta_x = 0.077 \pm 0.005 \text{ eV}, \tag{14a}$$
$$N_0\alpha - N_0\beta_z = 0.110 \pm 0.007 \text{ eV}, \tag{14b}$$

and for the $x = 0.92$ sample

$$N_0\alpha - N_0\beta_x = 0.089 \pm 0.005 \text{ eV}, \tag{15a}$$
$$N_0\alpha - N_0\beta_z = 0.126 \pm 0.007 \text{ eV}, \tag{15b}$$

where the uncertainties include the uncertainties in exciton transition energies and magnetization measurements. These values are an order of magnitude smaller than those observed for Mn-based II-VI DMS's as shown in Table IV. The exciton splitting, which is proportional to $N_0\alpha - N_0\beta$, is not an order of magnitude smaller but is ~ 3 times larger than that observed for II-VI DMS's. The larger exciton splitting is due to the ~ 30 times larger magnetization present in the $Cu_2Zn_{1-x}Mn_xGeS_4$ materials as measured at $B = 15$ T. The results of our experiments are not sufficient for determining the magnitudes and signs of $N_0\alpha$ and $N_0\beta$ separately.

The anisotropy of $N_0\beta$ is clearly evident in the optical data. The **E** || **c** exciton splitting is about 40% greater than the **E** || **a** splitting. For $x = 1.00$, $N_0\beta_z - N_0\beta_x = 0.033$ eV, and for $x = 0.92$, $N_0\beta_z - N_0\beta_x = 0.037$ eV. The relative size of the anisotropy depends on the magnitude

TABLE IV. $N_0\alpha - N_0\beta$ values for $Cu_2Zn_{1-x}Mn_xGeS_4$ and for several Mn-based II-VI DMS's.

DMS	$N_0\alpha - N_0\beta_x$ (eV)	$N_0\alpha - N_0\beta_z$ (eV)	$N_0\alpha - N_0\beta$ (eV)
$x = 1.00$	0.077 [a]	0.110 [a]	
$x = 0.92$	0.089 [a]	0.126 [a]	
$Cd_{1-x}Mn_xTe$			1.10 [b]
$Zn_{1-x}Mn_xTe$			1.28 [c]
$Cd_{1-x}Mn_xSe$	1.50 [d]	1.56 [d]	
$Zn_{1-x}Mn_xSe$			1.69 [e]

[a] This work.
[b] Reference 24.
[c] Reference 25.
[d] Reference 26.
[e] Reference 27.

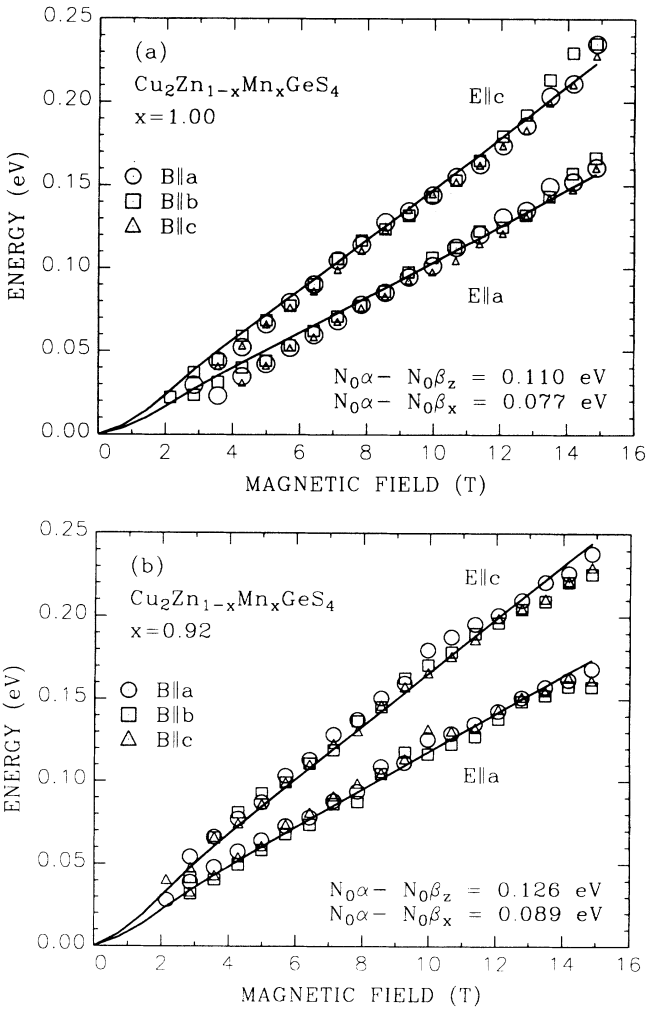

FIG. 8. Determination of *sp-d* exchange constants from fits to $Cu_2Zn_{1-x}Mn_xGeS_4$ optical splitting data. (a) $x = 1.00$. The **E** || **a** and **E** || **c** curves were calculated for $N_0\alpha - N_0\beta_x = 0.077$ eV and $N_0\alpha - N_0\beta_z = 0.110$ eV, respectively. (b) $x = 0.92$. The **E** || **a** and **E** || **c** curves were calculated for $N_0\alpha - N_0\beta_x = 0.089$ eV and $N_0\alpha - N_0\beta_z = 0.126$ eV, respectively.

of $N_0\beta$ about which we have no information. However we note that the anisotropy of $N_0\beta$ for $Cd_{1-x}Mn_xSe$ is less than 5% or $|N_0\beta_z - N_0\beta_x| = 0.064$ eV (Ref. 26). In absolute terms, the anisotropy observed in $Cd_{1-x}Mn_xSe$ is greater than that observed in $Cu_2Zn_{1-x}Mn_xGeS_4$.

Also, the values for $N_0\alpha - N_0\beta$ appear to vary strongly with x. In contrast, the II-VI DMS's with $x \lesssim 0.30$ exhibit constant $N_0\alpha - N_0\beta$ (Ref. 28). For $Cu_2Zn_{1-x}Mn_xGeS_4$, recall that the effective Mn concentration $x_{\text{eff}} = x/4$ does not exceed 0.25. As x increases by $\sim 9\%$ from $x = 0.92$ to 1.00, $N_0\alpha - N_0\beta_x$ decreases by 13.5% (or 0.012 eV) and $N_0\alpha - N_0\beta_z$ decreases by 12.7% (or 0.016 eV). This suggests that small changes in Mn concentration significantly change either the wavefunctions or the electrostatic interaction between the band and localized electrons. Another reason may be that second-order perturbation terms are important.[29] However, a calculation of this sort requires more detailed knowlege of the band structure.

Finally, Fig. 9 shows the average of the exciton transition energies as a function of magnetic field. The **E** || **c** average energy for all samples shows a 15–20 meV energy *increase* at 15 T while the **E** || **a** average energy shows a *decrease* of 20, 15, and 5 meV for the $x = 1.00$, 0.92, and 0.83 samples, respectively. In contrast, the II-VI DMS's exhibit an overall average energy increase due to the diamagnetic energy. We speculate that the heretofore neglected spin-orbit interaction causes the valence-band states to repel each other slightly such that the higher $|\mathcal{X}\rangle$ states move upward and the lower $|\mathcal{Z}\rangle$ states move downward. This would result in the observed shifts in average energy. A detailed quantitative calculation requires information about the $|\mathcal{Y}\rangle$ states which were unobserved in our experiments.

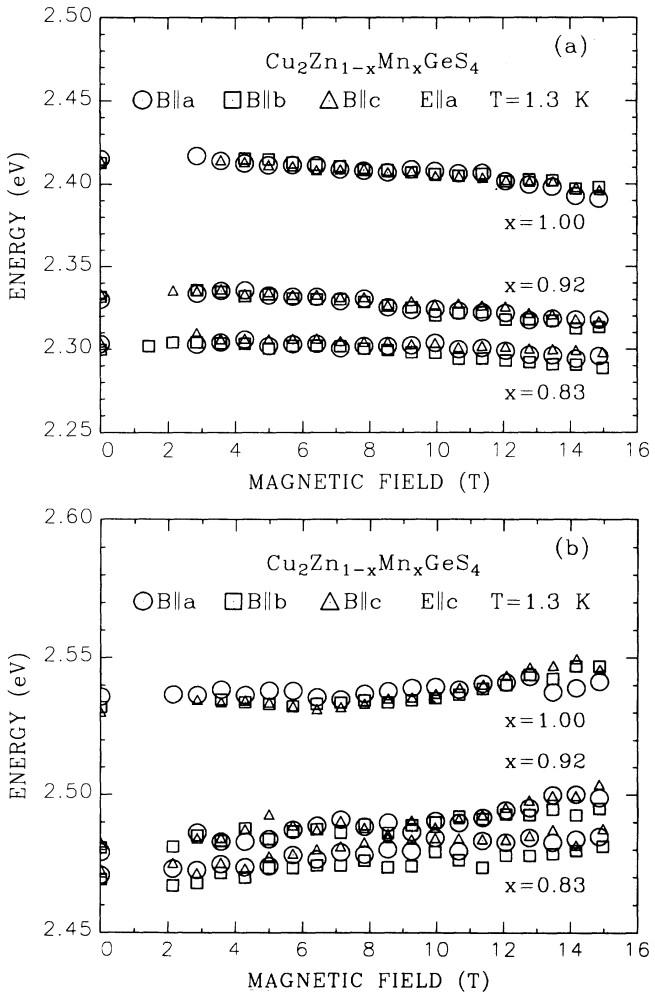

FIG. 9. $Cu_2Zn_{1-x}Mn_xGeS_4$ average energy of (a) **E** || **a** and (b) **E** || **c** exciton components. The **E** || **a** average energy decreases with B while the **E** || **c** average energy increases with B. The diamagnetic energy contribution would only increase the average energy.

V. SUMMARY

The *sp-d* exchange parameter difference $N_0\alpha - N_0\beta$ of orthorhombic wurtz-stannite $Cu_2Zn_{1-x}Mn_xGeS_4$ with $x = 0.92$ and 1.00 was determined from magnetoreflectance and magnetization data measured at $T \simeq 1.3$ and $0 \leq B \leq 19.5$ T. The conduction and valence bands were assumed to be *s*-like and *p*-like, respectively. Spin-orbit effects were considered negligible compared to the crystal-field splitting of the valence band. For both x concentrations and for both **E** || **a** and **E** || **c** polarizations, $N_0\alpha - N_0\beta \sim 0.1$ eV which is an order of magnitude smaller than that of Mn-based II-VI DMS's. However, the enhanced magnetization present in $Cu_2Zn_{1-x}Mn_xGeS_4$ more than compensates for the smaller $N_0\alpha - N_0\beta$ which results in *larger* magneto-optical effects than those observed in II-VI DMS's. The exciton splittings were a factor of 3 larger at $B = 15$ T. Larger *sp-d* exchange parameters could possibly be found among DMS's derived from other I_2-II-IV-VI_4 compounds having other magnetic ions.

Additionally, room-temperature excitons were observed but their Zeeman splittings were not observed for $B \leq 15$ T. Conceivably, room-temperature exciton splittings could be observed in larger magnetic fields with better quality crystals having narrower exciton line widths. Also, the crystal-field splittings measured at $B = 0$ were larger for smaller x. This was correlated with the increasing distortion of the crystal lattice away from the ideal wurtzite lattice. Finally, the average energy of the **E** || **a** exciton transitions was found to decrease with increasing magnetic field while that of the **E** || **c** exciton transitions increased. In II-VI DMS's, the diamagnetic energy contribution always causes the average energy to increase with magnetic field.

ACKNOWLEDGMENTS

We thank Professor M. Kastner and Professor J. Joannopoulos for some helpful discussions. This work was supported by National Science Foundation Grant No. DMR-8807419. The Francis Bitter National Magnet Laboratory is supported by National Science Foundation cooperative agreement No. DMR-8813164.

APPENDIX

Here we present our description of a crystal plane in a Cartesian coordinate system that differs from Eq. (6.1) in Ref. 18. The crystal plane is characterized by Miller indices $h'k'l'$ and hkl in crystal and Cartesian coordinate systems $X'Y'Z'$ and $\xi\eta\zeta$, respectively. A crystal plane having Miller indices $h'k'l'$ intercepts the $X'Y'Z'$ axes at the three points $(a/h', 0, 0)$, $(0, b/k', 0)$, and $(0, 0, c/l')$ where a, b, and c are the lattice constants. These three points may be reexpressed in terms of the coordinates (ξ, η, ζ) and the angles $\gamma, \delta, \beta, \psi, \epsilon$ as defined in Fig. 6.2 in Ref. 18. They are

$$\left(\frac{a}{h'}, 0, 0\right) \rightarrow (\xi_1, \eta_1, \zeta_1) = \left(\frac{a}{h'}, 0, 0\right), \tag{A1}$$

$$\left(0, \frac{b}{k'}, 0\right) \rightarrow (\xi_2, \eta_2, \zeta_2) = \left(\frac{b}{k'}\cos\gamma, \frac{b}{k'}\cos\delta, 0\right), \tag{A2}$$

$$\left(0, 0, \frac{c}{l'}\right) \rightarrow (\xi_3, \eta_3, \zeta_3) = \left(\frac{c}{l'}\cos\beta, \frac{c}{l'}\cos\psi, \frac{c}{l'}\cos\epsilon\right). \tag{A3}$$

These three points in the $\xi\eta\zeta$ system determine the plane whose equation is given by[30]

$$\begin{vmatrix} \xi & \eta & \zeta & 1 \\ \xi_1 & \eta_1 & \zeta_1 & 1 \\ \xi_2 & \eta_2 & \zeta_2 & 1 \\ \xi_3 & \eta_3 & \zeta_3 & 1 \end{vmatrix} = 0. \tag{A4}$$

Thus a plane in the $X'Y'Z'$ coordinate system has been expressed in terms of the (ξ, η, ζ) coordinates.

Finally, the Miller indices hkl are the reciprocals of the intercepts the plane makes with the $\xi\eta\zeta$ axes. The intercepts are found by setting two of the (ξ, η, ζ) variables in Eq. (A4) to zero and solving for the remaining variable. The hkl indices are given as follows:

$$h = h'/a, \tag{A5a}$$

$$k = [(k'/b) - (h'/a)\cos\gamma]/\cos\delta, \tag{A5b}$$

$$l = [(l'/c)\cos\delta + (h'/a)(\cos\gamma\cos\psi - \cos\delta\cos\beta) - (k'/b)\cos\psi]/(\cos\epsilon\cos\delta). \tag{A5c}$$

Also, according to our derivation, Eq. (6.8) in Ref. 18 should read

$$\varphi = \mathrm{sgn}(\mathbf{g}\cdot\mathbf{v})\cos^{-1}(\mathbf{g}\cdot\mathbf{s}/\cos\theta). \tag{A6}$$

---

*Also at Lincoln Laboratory, Massachusetts Institute of Technology, Lexington, MA 02173.

†Also at Francis Bitter National Magnet Laboratory, Massachusetts Institute of Technology, Cambridge, MA 02139.

‡Present address: Naval Research Laboratory, Washington, D.C. 20375.

[1] *Semiconductors and Semimetals*, edited by R. K. Willardson and A. C. Beer (Academic, New York, 1988), Vol. 25.

[2] Y. Shapira, J. Appl. Phys. **67**, 5090 (1990).

[3] X. Wang, D. Heiman, S. Foner, and P. Becla, Phys. Rev. B **41**, 1135 (1990).

[4] E. D. Isaacs, D. Heiman, X. Wang, P. Becla, K. Nakao, S. Takeyama, and N. Miura, Phys. Rev. B **43**, 3351 (1991).

[5] D. Heiman, E. D. Issacs, P. Becla, and S. Foner, in *Diluted Magnetic (Semimagnetic) Semiconductors*, Materials Research Society Symposia Proceedings, edited by R. L. Aggarwal, J. K. Furdyna, and S. von Molnar (Materials Research Society, Pittsburgh, 1987), Vol. 89, p. 21.

[6] P. A. Wolff and L. R. Ram-Mohan, in *Diluted Magnetic (Semimagnetic) Semiconductors*, Materials Research Society Symposia Proceedings, edited by R. L. Aggarwal, J. K. Furdyna, and S. von Molnar (Materials Research Society, Pittsburgh, 1987), Vol. 89, p. 1.

[7] E. Parthé, *Crystal Chemistry of Tetrahedral Structures* (Gordon and Breach, New York, 1964).

[8] R. Nitsche, D. F. Sargent, and P. Wild, J. Cryst. Growth **1**, 52 (1967).

[9] E. Parthé, K. Yvon, and R. H. Deitch, Acta Crystallogr. Sect. B **25**, 1164 (1969).

[10] W. Schäfer and R. Nitsche, Mater. Res. Bull. **9**, 645 (1974).

[11] Y. Shapira, E. J. McNiff, Jr., N. F. Oliveira, Jr., E. D. Honig, K. Dwight, and A. Wold, Phys. Rev. B **37**, 411 (1988).

[12] D. M. Schleich and A. Wold, Mat. Res. Bull. **12**, 111 (1977).

[13] L. K. Samanta and G. C. Bhar, Phys. Status Solidi A **41**, 331 (1977).

[14] L. Guen, W. S. Glaunsinger, and A. Wold, Mat. Res. Bull. **14**, 463 (1979).

[15] L. Guen and W. S. Glaunsinger, J. Solid State Chem. **35**, 10 (1980).

[16] K. Ito and T. Nakazawa, Jpn. J. Appl. Phys. **27**, 2094 (1988).

[17] E. Honig, H-S. Shen, G-Q. Yao, K. Doverspike, R. Kershaw, K. Dwight, and A. Wold, Mat. Res. Bull. **23**, 307 (1988).

[18] E. Preuss, B. Krahl-Urban, and R. Butz, *Laue Atlas* (Wiley, New York, 1974), p. 60.

[19] J. L. Shay, B. Tell, L. M. Schiavone, H. M. Kasper, and F. Thiel, Phys. Rev. B **9**, 1719 (1974).

[20] R. L. Aggarwal, S. N. Jasperson, J. Stankiewicz, Y. Shapira, S. Foner, B. Khazai, and A. Wold, Phys. Rev. B **28**, 6907 (1983).

[21] O. W. Shih, R. L. Aggarwal, Y. Shapira, S. H. Bloom,

V. Bindilatti, R. Kershaw, K. Dwight, and A. Wold, Solid State Commun. **74**, 455 (1990).
[22] M. Nawrocki, F. Hamdani, J. P. Lascaray, Z. Golacki, and J. Deportes, Solid State Commun. **77**, 111 (1991).
[23] D. L. Dexter and R. S. Knox, *Excitons* (Interscience, New York, 1965), p. 53.
[24] J. A. Gaj, R. Planel, and G. Fishman, Solid State Commun. **29**, 435 (1979).
[25] A. Twardowski, P. Swiderski, M. von Ortenberg, and R. Pauthenet, Solid State Commun. **50**, 509 (1984).
[26] M. Arciszewska and M. Nawrocki, J. Phys. Chem. Solids **47**, 309 (1986).
[27] A. Twardowski, T. Dietl, and M. Demianiuk, Solid State Commun. **48**, 845 (1983).
[28] J. P. Lascaray, M. C. D. Deruelle, and D. Coquillat, Phys. Rev. B **35**, 675 (1987).
[29] A. K. Bhattacharjee, Solid State Commun. **65**, 275 (1988).
[30] C. O. Oakley, *Analytic Geometry* (Barnes and Noble, New York, 1957).